# Highly viscoelastic films at the water/air interface: α-Cyclodextrin with anionic surfactants

Alberto S. Luviano [a,b], Jorge Hernández-Pascacio [a], Daniel Ondo [c], Richard A. Campbell [d,e,*], Ángel Piñeiro [f,*], José Campos-Terán [b,g,*], Miguel Costas [a,*]

[a] *Laboratorio de Biofisicoquímica, Departamento de Fisicoquímica, Facultad de Química, Universidad Nacional Autónoma de México, CdMx 04510, Mexico*
[b] *Departamento de Procesos y Tecnología, Universidad Autónoma Metropolitana, Unidad Cuajimalpa, Av. Vasco de Quiroga 4871, Col. Santa Fe, Delegación Cuajimalpa de Morelos, 05348, CdMx, Mexico*
[c] *Department of Physical Chemistry, University of Chemistry and Technology, Technická 5, 166 28 Prague 6, Czech Republic*
[d] *Institut Laue-Langevin, 71 avenue des Martyrs, 38042 Grenoble, France*
[e] *Division of Pharmacy and Optometry, University of Manchester, Manchester M13 9PT, United Kingdom*
[f] *Departamento de Física de Aplicada, Facultade de Física, Universidade de Santiago de Compostela, E-15782 Santiago de Compostela, Spain*
[g] *Lund Institute of Advanced Neutron and X-ray Science, Lund University, Scheelevägen 19, 223 70 Lund, Sweden*

## GRAPHICAL ABSTRACT
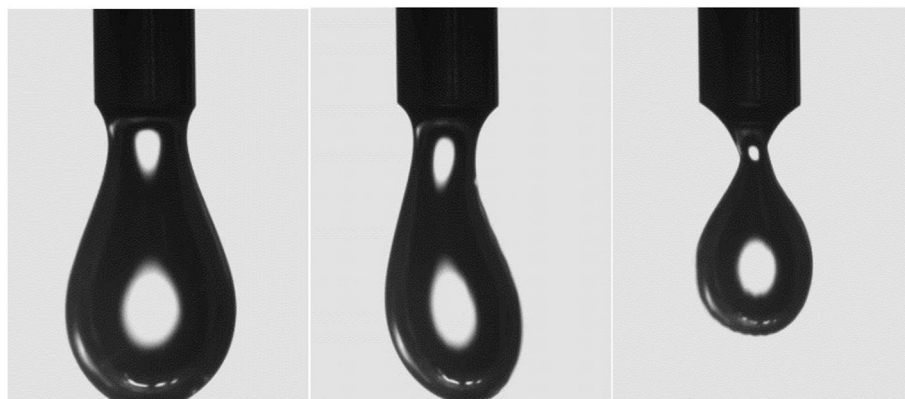


## ARTICLE INFO

## ABSTRACT

This work showcases the remarkable viscoelasticity of films consisting of α-cyclodextrin (α-CD) and anionic surfactants (S) at the water/air interface, the magnitude of which has not been observed in similar systems. The anionic surfactants employed are sodium salts of a homologous series of *n*-alkylsulfates (*n* = 8–14) and of dodecylsulfonate. Our hypothesis was that the very high viscoelasticity can be systematically related to the bulk and interfacial properties of the system. Through resolution of the bulk distribution of species using isothermal titration calorimetry, the high dilatational modulus is related to $(\alpha\text{-CD})_2$:$S_1$ inclusion complexes in the bulk with respect to both the bulk composition and temperature. Direct interfacial characterization of α-CD and sodium dodecylsulfate films at 283.15 K

using ellipsometry and neutron reflectometry reveals that the most viscoelastic films consist of a highly ordered monolayer of 2:1 complexes with a minimum amount of any other component. The orientation of the complexes in the films and their driving force for adsorption are discussed in the context of results from molecular dynamics simulations. These findings open up clear potential for the design of new functional materials or molecular sensors based on films with specific mechanical, electrical, thermal, chemical, optical or even magnetic properties.

## 1. Introduction

Native cyclodextrins (CDs) are cyclic oligosaccharides that result from the enzymatic degradation of starch and have interesting structural, chemical and physicochemical properties [1]. They are formed by six ($\alpha$-CD), seven ($\beta$-CD), or eight ($\gamma$-CD) 1,4-linked $\alpha$-D-glucopyranoside units. Their molecular crystal structure indicates a truncated cone shaped geometry although they are highly flexible in aqueous solution [2,3]. The external surface of the CDs is hydrophilic rendering them water soluble, while their internal cavity, which increases in size from $\alpha$- to $\gamma$-CD, is hydrophobic and hence able to host hydrophobic molecules such as surfactants, lipids, drugs, amino acids, polymers, and dyes [4–9]. Stemming from this ability of CDs to increase the solubility of hydrophobic moieties in so-called inclusion complexes, together with their low toxicity, a huge number of research articles has been published and thousands of CD-based patents have been registered [10], with many of them being commercially exploited. All these reports cover a large number of fields such as biomedicals, pharmaceuticals, food technology, cosmetics, agrochemistry, biological sensors, environmental protection, membranes, and electrochemistry [11–19]. In bulk aqueous solution CDs exist in the form of spontaneously formed aggregates bound together by a network of hydrogen bonds where water molecules play an important role [3,20–24]. While $\alpha$-CD monomers are not surface active [25–27], we have shown recently that $\alpha$-CD aggregates formed in the bulk solution adsorb spontaneously to the water/air interface, forming two-dimensional domains on the $\mu$m size scale with a layer thickness of ~4 nm [27].

The bulk and surface properties of aqueous cyclodextrin/surfactant mixtures have been extensively studied with a variety of techniques [28,29]. As for their bulk properties, the thermodynamic characterization of the host-guest binding process has been experimentally determined for many systems [30] and, in particular, for some of the systems linked to the present work [31,32]. Also, molecular dynamics (MD) simulations have been employed to study inclusion complexes [33–37]. As for their surface properties, in particular the surface rheological behavior, both the dilatational and shear rheology [38,39], have proven to be very useful in enhancing the understanding of the nature of adsorbed films composed of long semifluorinated alkanes [40], fluoro-alkyl phosphates [41] and protein systems [42], with applications in many areas ranging from medical diagnostics [39] to oil recovery [43]. However, the role of the inclusion complexes in the rheological behavior of materials adsorbed at the water/air interface has been the subject of only a limited number of reports. For example, the surface tension of host-guest complexes has been examined for $\alpha$-CD with cationic-anionic hydrogenous and fluorinated surfactants [44], while the dilatational rheological behavior has been studied both for $\beta$-CD with a cationic surfactant [45] and for $\alpha$-CD with the anionic surfactant sodium dodecylsulfate ($C_{12}SO_4^-$) [25,26]. In the latter case the spontaneously formed film at the water/air interface displays a remarkable viscoelasticity, one order of magnitude larger than typical amphiphilic molecules.

The aims of the present work are to examine the influence of factors that affect the surface rheological behavior of {surfactant + $\alpha$-CD} systems at the water/air interface, and gain insight into its underlying physical basis. In this context, we have measured the dilatational modulus as a function of surfactant concentration, alkyl chain length and temperature. These data are rationalized using the distribution of species in the bulk solutions obtained using isothermal titration calorimetry. Also, for {$C_{12}SO_4^-$ + $\alpha$-CD} mixtures at 283.15 K, we have characterized the interfacial adsorption and structures created in films of different bulk compositions and varying viscoelasticity through the application of complementary surface-sensitive techniques, ellipsometry and neutron reflectometry. The results are discussed in the context of insight from MD simulations. Our approach is based on a bottom-up strategy – design of devices with specific macroscopic properties based on the control of molecular level structures [46] – and takes advantage of the ability of CDs to encapsulate different compounds with specific stoichiometry and affinity with a view to the potential development of new films for specific applications.

## 2. Experimental section

### 2.1. Materials

Surfactants (sodium salts) octylsulfate ($C_8SO_4^-$, purity >99%), decylsulfate ($C_{10}SO_4^-$, purity >99%), fully protonated dodecylsulfate (h-$C_{12}SO_4^-$, purity >99%), dodecylsulfonate ($C_{12}SO_3^-$, purity >99%), tetradecylsulfate ($C_{14}SO_4^-$, purity >95%), $\alpha$-cyclodextrin ($\alpha$-CD, purity >98%) and deuterated water ($D_2O$, purity 99.99%) were obtained from Sigma-Aldrich. Fully deuterated d-$C_{12}SO_4^-$ (purity >98%) was obtained from Cambridge Isotopes. Ultra-pure water with a resistivity of 18.2 M$\Omega$ cm was obtained from a Millipore system. The water content of $\alpha$-CD was 10% by weight, as determined by Karl Fischer titration. All materials were used without further purification.

### 2.2. Sample preparation

For the dilatational modulus, ellipsometry and neutron reflectometry experiments, {surfactant + water} and {$\alpha$-CD + water} stock solutions were carefully prepared by weight (correcting for $\alpha$-CD water content) at twice the final desired concentration. Prior to mixing the stock solutions they were heated at 323.15 K for 30 min and sonicated for 15 min to guarantee complete solubilization. Equal volumes of these stock solutions were mixed to provide the expected $r$ = [surfactant]/[$\alpha$-CD] ratio. In all cases, the final surfactant concentrations were below the critical micelle concentration (CMC) in the presence of $\alpha$-CD [47,48]. For all the techniques employed, samples were pipetted from the bulk to the measurement cell or troughs to avoid the transfer of kinetically trapped material formed at the water/air interface during its creation [49]. Adequate volumes were prepared so that the same sample was used for both ellipsometry and neutron reflectometry experiments.

## 2.3. Dilatational modulus (E)

The surface tension and dilatational rheology of the adsorbed material at the water/air interface were measured by the pendant drop technique using an image drop profile tensiometer (OCA20, Dataphysics, Germany) equipped with a piezoelectric oscillating module (ODG20, Dataphysics, Germany), a high-resolution CCD camera (max 123 fps) and a home-designed thermostatized cell constructed with optic glass by Hellma, Germany (see Part 1 of the Supplementary Material). This cell allows measurements for up to 24 h at constant temperature with low evaporation rate. Drops of 18–20 μL were created from a 500 μL syringe with a stainless steel needle. The measurements were performed at 283.15 and 293.15 K (±0.1 K), the temperature being controlled using a Haake (K20, Thermo Scientific) bath. The drop profiles were captured by CCD camera, and the images analyzed by solving the Young-Laplace equation to obtain the surface tension ($\gamma$) and interfacial area ($A$). Through repetition of the measurements, the accuracy is estimated to be 0.2 mN/m for the surface tension.

To study the interfacial dilatational rheological properties of the systems, sinusoidal periodic oscillation experiments were performed with an area deformation ($\Delta A$) of ~6% and a linear frequency (f) sweep from 0.01 to 0.20 Hz (five frequencies equally spaced in this interval). All the measurements were performed in the linear viscoelastic regime (see Part 2 of the Supplementary Material). Prior to being oscillated, the pendant drops in the measurement cell were left unperturbed for 90 min. This is the time necessary for the film formed at the water/air interface to reach equilibrium, i.e. for $\gamma$ to become constant. Upon oscillation, the drop area change produces a variation of the surface tension which is characterized by the dilatational modulus $|E| = d\gamma/d\ln A$. The elastic ($E'$) and viscous ($E''$) contributions are defined by the phase change ($\delta$) between the area and interfacial sinusoidal oscillations. A purely elastic behavior is characterized by $\delta = 0°$ while for a purely viscous behavior $\delta = 90°$. At each experimental condition (concentration and temperature) at least three different drops were measured, providing the standard deviation for the $E$ values. Essentially the same results were found in a Langmuir trough regarding the surface tension, which gave similar $E$ values within the experimental uncertainty (see figures in Part 3 of the Supplementary Material). Since drop measurements require much less sample volume and are easier to perform repetitions, all the measurements reported here were done using the pendant drop technique.

## 2.4. Isothermal titration calorimetry (ITC)

The interactions between surfactants and α-CD in bulk aqueous media were studied using an ultrasensitive power compensating isothermal titration microcalorimeter (VP-ITC MicroCal, Northampton, USA). The aqueous solutions were prepared by weight taking into account the water content present in α-CD, and were duly degassed prior to placing them in the cell and syringe. The surfactant and α-CD aqueous solutions were placed in the calorimeter syringe and cell, respectively. The measured heats were corrected for the corresponding dilution heats of the surfactant titrated into pure solvent.

For four of the five surfactants employed here, the results have been presented and discussed previously [31,32]. In the present work, the interaction of $C_{14}SO_4^-$ with α-CD was studied at four temperatures (283.15, 293.15, 303.15 and 313.15 K) on a calorimeter equipped with a cell of 1.4524 mL reaction volume and a 282-μL syringe. The CMC of $C_{14}SO_4^-$ in water at 318.15 K was measured as described in the literature [50], by injecting 28 mM surfactant solution into pure water solvent (56 injections of 5 μL). The inflexion point on the titration curve, i.e. the CMC, was found to be

1.15 mM. An α-CD solution (0.2 mM) placed in the cell was titrated with a $C_{14}SO_4^-$ surfactant solution below the CMC (1.0 mM) placed in the syringe. The titrations consisted of first a blank 1 μL injection, followed by 28 injections of 10 μL, with a 6 min delay between them and stirring of the cell content at 437 rpm. The raw heatflow data were processed using the ITC data analysis program provided by MicroCal. In order to obtain the thermodynamic parameters (equilibrium constant, enthalpy and heat capacity changes) for the α-CD/$C_{14}SO_4^-$ interaction, data were processed using a multi-temperature fitting procedure [32] described in detail in Part 4 of the Supplementary Material.

The interactions of fully protonated h-$C_{12}SO_4^-$ and fully deuterated d-$C_{12}SO_4^-$ with α-CD were studied at 283.15 K on a different calorimeter equipped with a cell of 1.4196 mL reaction volume and a 279-μL syringe. α-CD solutions (0.5 and 1.0 mM) placed in the cell were titrated with h-$C_{12}SO_4^-$ and d-$C_{12}SO_4^-$ solutions (5.0 mM) placed in the syringe. Titrations consisted of first a blank 2 μL injection, followed by 14 injections of 5 μL, and after by 22 injections of 10 μL, with a 10 min delay between them and stirring of the cell content at 450 rpm. Using the same procedure, the interactions of α-CD (0.5 and 1.0 mM) with h-$C_{12}SO_4^-$ and d-$C_{12}SO_4^-$ in $D_2O$ were also studied. The molality of the solutions was converted to molarity by approximating the density of the solution to the density of pure $D_2O$ solvent [51] The interaction of α-CD with h-$C_{12}SO_4^-$ in water was described in our previous reports [31,32]. A global fitting of the four systems (α-CD with two surfactants in two solvents) using the software AFFINImeter [52] was performed.

## 2.5. Ellipsometry (EP)

EP data were recorded using a Picometer Light phase modulated ellipsometer (Beaglehole Instruments, New Zealand) in the Partnership for Soft Condensed Matter (Grenoble, France) with a sampling frequency of 0.2 Hz. The instrument was equipped with a He-Ne laser of $\lambda = 633$ nm using an angle of incidence $\theta = 50°$, close to Brewster angle of the interface. The technique probes the change in polarization of light upon reflection, where the phase shift ($\Delta$) is most sensitive to the presence of an interfacial layer; the amplitude change ($\Psi$) is relatively insensitive to the interfacial layer and so was ignored in the present work [53]. The data are presented as $\Delta_{surf} = \Delta - \Delta_0$, where $\Delta_{surf}$ is the change in $\Delta$ resulting from the adsorbed layer at the interface, $\Delta$ is the measured value and $\Delta_0$ is the reference value for pure water. This subtraction process minimizes effects on the data from surface roughness [54].

Although in principle an optical matrix model may be applied to the data to convert values of $\Delta_{surf}$ into the surface excess, the difficulties of its application in the present work cannot be understated. Even if an average refractive index were used for the species at the interface, the molecular orientations have not been unambiguously resolved, and therefore strong anisotropic contributions from the ordered adsorption of α-CD/surfactant complexes or even monolayer domains of pure surfactant would be left unquantified. As such, the purpose of the measurements was to acquire information about the approximate extent of adsorption at the interface, the adsorption kinetics, and the lateral homogeneity of the resulting layer from the presence of temporal fluctuations in the data [55], as seen by the obtained values of $\Delta_{surf}$.

## 2.6. Neutron reflectometry (NR)

The experiments were performed on the time-of-flight reflectometer FIGARO [56] at the Institut Laue-Langevin (Grenoble, France). Profiles of the neutron reflectivity $R$ at the water/air interface as a function of the momentum transfer $q = 4\pi \sin(\theta)/\lambda$ were recorded at 283.15 K using neutron pulses in the wavelength range $\lambda = 2$–30 Å and at fixed incident angles of $\theta = 0.62°$ and 3.8°. The

principles of the technique, features of its application at the water/air interface and the specific 'adsorption troughs' setup for measurements at low temperatures used for our experiments have been described recently [57]. Two executions of the technique were performed: the first sensitive to the interfacial composition and the second sensitive to the interfacial structure; information about the various models applied to fit the data and the fitting parameter calculations can be found in Part 5 of the Supplementary Material.

The low-$q$ interfacial composition analysis method [57] was first used to resolve the surface excesses of α-CD and $C_{12}SO_4^-$ for equilibrated samples over the full range of bulk compositions studied. Measurements were made of {h-$C_{12}SO_4^-$ + α-CD} and {d-$C_{12}SO_4^-$ + α-CD} in air contrast matched water (ACMW; a mixture of 8.1% by volume of $D_2O$ in $H_2O$, which is transparent to neutrons). The former isotopic contrast is sensitive primarily to the presence of α-CD at the interface while the latter contrast is sensitive primarily to the surfactant. Data were reduced in a restricted $q$-range of 0.01–0.03 Å$^{-1}$ to minimize sensitivity of the analysis to the interfacial structure. The scattering contribution from the interfacial material is presented as the product of scattering length density ($\rho$) and thickness ($d$) in the applied single-layer model. The data were analyzed using the batch fit application of Motofit [58].

A structural analysis method was then applied. For these measurements, solutions of {h-$C_{12}SO_4^-$ + α-CD} and {d-$C_{12}SO_4^-$ + α-CD} were prepared in two different isotopic contrasts of the solvent: ACMW and $D_2O$. Information evidencing the applicability of a global fit to the data recorded in different isotopic contrasts can be found in Part 5 of the Supplementary Material. The data were analyzed using SANGRA (Script Automated Neutron Grazing Reflectivity Analysis), a home-made program [27] based on the implementation of the Parratt method [59] for the modeling of homogeneous stratified layers by using the Fresnel equations. Also implemented in this program is an option to model domains of different composition with sizes above the coherence length, which varies from ∼ 100 μm at low $q$ (dominating the surface excess) to ∼ 10 μm at high $q$ (dominating the structural analysis) [60]. A homogenous single-layer model was found to fit well the experimental data. Alternative models involving the simultaneous adsorption of α-CD and h/d-$C_{12}SO_4^-$ in multiple layers, and another involving the formation of lateral domains in the plane of the surface (above the coherence length of the probe), were also attempted, but it was found that either they were unable to fit the data or the number of fitting parameters required was not statistically justified.

## 3. Results and discussion

### 3.1. Effects of surfactant chain length, surfactant head group and bulk composition

Values of the dilatational modulus ($E$) for α-CD/surfactant mixtures at 283.15 K as a function of the concentration ratio $r$ = [surfactant]/[α-CD] are shown for the five different anionic surfactants considered in the present study in Fig. 1A. For the shorter alkyl chain surfactant $C_8SO_4^-$ the viscoelasticity is very small and equal to the values obtained for the {surfactant + water} and {α-CD + water} binary mixtures ($E \cong 10$ mN/m). On the other hand, for longer chain surfactants the viscoelasticity exhibits a maximum at $r$ = 0.310 and $E \cong 100$ mN/m for $C_{10}SO_4^-$, at $r$ = 0.340 and $E \cong 150$ mN/m for $C_{12}SO_4^-$, and at $r$ = 0.410 and $E \cong 280$ mN/m for $C_{14}SO_4^-$. The 10 to 28-fold increase in the viscoelasticity found for these three {surfactant + α-CD + water} ternary mixtures is a clear indication that the spontaneously adsorbed material at the water/air interface generates a highly viscoelastic film. The viscoelastic
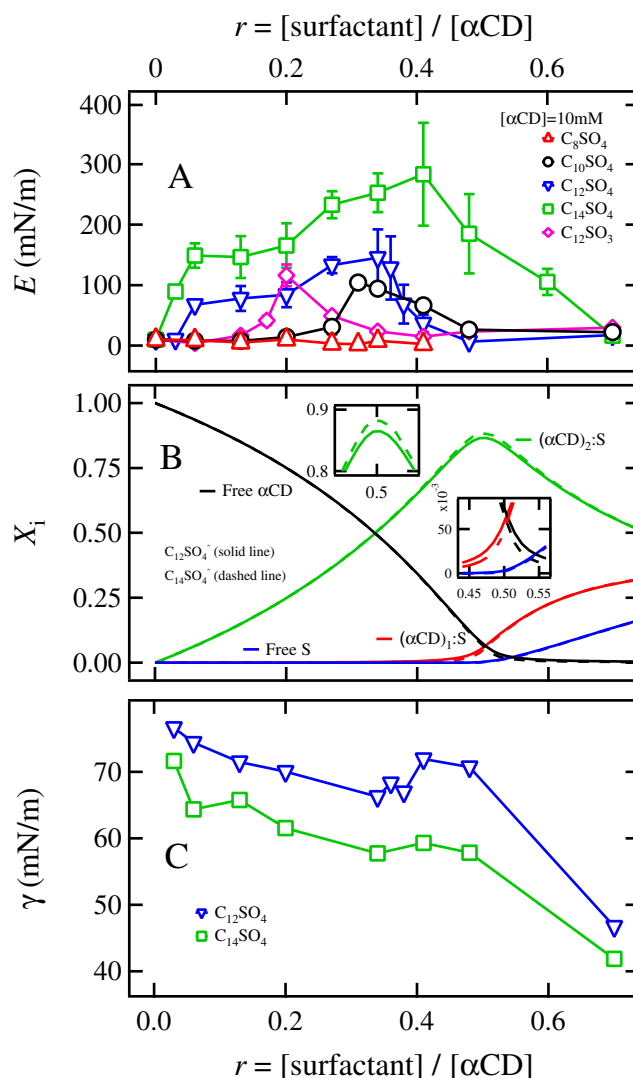


**Fig. 1.** (A) Dilatational modulus ($E$) for five anionic surfactants at 283.15 K as a function of the concentration ratio $r$ = [surfactant]/[α-CD]. In these experiments, the concentration of α-CD was kept constant and equal to 10 mM and the frequency of the sinusoidal periodic oscillation was 0.20 Hz. The error bars are the standard deviations obtained from the measurements of at least three different drops. (B) Distribution of species at 283.15 K in the bulk solution for $C_{12}SO_4^-$ and $C_{14}SO_4^-$ at 283.15 K obtained from ITC measurements in ref. [32] and this work, respectively. The distribution of species for the other three surfactants can be found in Part 8 of the Supplementary Material. (C) Surface tension for {$C_{12}SO_4^-$ + 10 mM α-CD} and {$C_{14}SO_4^-$ + 10 mM α-CD} at 283.15 K.

behavior of this film is remarkable as it can be appreciated in the video for the $C_{14}SO_4^-$ system (see Part 6 of the Supplementary Material). In the literature [61–65], for a broad variety of systems involving hydrocarbon surfactants, most of the reported $E$ values are smaller than 50 mN/m (in the frequency range 0.005 to 0.2 Hz and at temperatures above 293.15 K) with the exception of 24 h aged aqueous solutions of $C_{12}SO_4^-$ in the presence of divalent salts [66] at 293.15 K (maximum of 90 mN/m) and two hydroxyl substituted alkyl benzenesulfonates in water [67] at 303.15 K (maximum of 100 mN/m). On the other hand, very large $E$ values for aqueous fluoro-alkyl phosphates and protein systems have been published [41,42,68]. The only surface viscoelasticity measurements for CD-based systems available in the literature corresponds to the mixture of β-CD with cetyltrimethylammonium bromide that shows a maximum $E$ value of 25 mN/m at 298.15 K [45]. Clearly, most of the $E$ values in Fig. 1A are bigger than those

reported in the literature, which emphasizes the notable viscoelastic behavior of the CD-based systems studied here.

At 283.15 K and the $r$ value where the $E$ maximum occurs, the elastic contribution to the elastic modulus ($E'$) is lower or equal to the viscous contribution ($E''$) for the five employed oscillation frequencies (see Part 7 of the Supplementary Material) for $C_{10}SO_4^-$ and $C_{14}SO_4^-$. In contrast, $E' \cong E''$ to within the experimental uncertainty for $C_{12}SO_3^-$. However, for $C_{12}SO_4^-$ there is a crossover point occurring at approximately 0.05 Hz ($E'<E''$ below 0.10 Hz; and $E'>E''$ above 0.10 Hz) between the viscous and the elastic contributions. To the best of our knowledge this crossover behavior has not been reported in dilatational rheology studies, but rather for shear rheology of Maxwellian fluids like polyelectrolyte/surfactant mixtures [69] and non-Maxwellian fluids [70,71]. Finally, in Fig. 1A the viscoelasticity does not show a saturation-type trend with increasing $r$ but rather it decreases towards very low $E$ values.

Since the spontaneously formed species in the bulk solution are typically closely connected with those present at the water/air interface, our working hypothesis is that the viscoelasticity data in Fig. 1A may be rationalized in terms of the distribution of chemical species in the bulk i.e. the concentrations of free components and the inclusion complexes formed between α-CD and the surfactant (S). This information can be obtained from ITC experiments that provide the thermodynamic parameters (equilibrium constants and enthalpies) reported in Table 1 for the five studied surfactants, corresponding to the formation of the 1:1 and 2:1 inclusion complexes, α-CD:S and (α-CD)$_2$:S, respectively. The species distribution as a function of $r$ = [S]/[α-CD] can be easily obtained from the equilibrium constants using the simulation tool freely available in the AFFINImeter software [52].

The corresponding results for $C_{12}SO_4^-$ and $C_{14}SO_4^-$ at 283.15 K are plotted in Fig. 1B, showing that the distribution of species for these two surfactants are practically identical (the distribution of species for the five surfactants can be seen in Part 8 of the Supplementary Material). In the $r$ interval where the film at the water/air interface shows a remarkable viscoelastic behavior, the bulk is generally populated by 2:1 complexes and free α-CD (with a minimal amount of 1:1 complexes and free S). An exception is the {$C_{14}SO_4^-$ + α-CD} system where the viscoelasticity persists to higher $r$ values and there is a notable increase of 1:1 complexes with free S and negligible free α-CD. The only common species which links the high viscoelasticity for all the systems and $r$ values is the presence of 2:1 complexes in the bulk. For instance, at $r$ = 0.340 and $r$ = 0.410 where $E$ is maximum for $C_{12}SO_4^-$ and $C_{14}SO_4^-$, respectively, the distribution of species in the bulk is approximately 50% of 2:1 complexes and 49% of free α-CD for $C_{12}SO_4^-$, and 68% of 2:1 complexes and 31% of free α-CD for $C_{14}SO_4^-$.

The link between the presence of 2:1 complexes in the bulk and the high viscoelasticity of the systems may be placed in the context of previous results from MD simulations where it was found that α-CD monomers are not surface-active [3] while the affinity of individual 2:1 complexes to the interface is high [25]. These observations link the adsorption of 2:1 complexes at the water/air interface to the high viscoelasticity of the system, although from these data alone it is not possible to say whether aggregates of α-CD, which are known to exist in the bulk and adsorb to the water/air interface over time [27], have an effect on the viscoelasticity of the system. A comparison of Fig. 1A and 1B indicates that for $C_{12}SO_4^-$ and $C_{14}SO_4^-$ the $r$ region at which $E$ starts to decrease coincides with an increase in the concentration of 1:1 complexes, which could be related to the competition at the interface with the 2:1 complexes (if the 1:1 complexes are surface-active) or a simple reduction in concentration in the bulk and therefore at the interface of the 2:1 complexes (if the 1:1 complexes are not surface-active). Then with further increasing $r$, the concentration of free surfactant in the bulk and the amount present at the interface increase, and the system does not exhibit high viscoelasticity ($E \cong 10$ mN/m). Lastly, Fig. 1A shows that a subtle change in the polar head of the surfactant, i.e. in going from $C_{12}SO_4^-$ to $C_{12}SO_3^-$, produces a decrease of the viscoelasticity maximum (from $E \cong 150$ mN/m to $E \cong 115$ mN/m) and of the $r$ value (from $r$ = 0.340 to $r$ = 0.200) at which it occurs. Clearly, the effect of removing the oxygen atom linking the alkyl chain with the sulfur atom is substantial, and indicates that the surfactant polar head is importantly involved in the bulk interactions leading to the species distribution (see Part 8 of the Supplementary Material).

If we consider surfactant alkyl chain length, a comparison of Fig. 1A and 1B shows that the films formed with $C_{12}SO_4^-$ and $C_{14}SO_4^-$ do not show the same viscoelasticity, despite having almost the same amount of 2:1 complexes in their bulk solution across the whole range of $r$ values. It follows that the magnitude of $E$ is system-dependent and is determined not only by the composition of species in the bulk but from other interfacial factors. To explore this effect, the surface tension values associated with the two systems are displayed with respect to $r$ in Fig. 1C. Here, a clear link is shown between the lower surface tension and higher $E$ values for the system with the longer surfactant chains. It can be inferred from these data that the high viscoelasticity values for these systems is also related to the different affinity for the interface of the bulk species, resulting in different adsorbed amounts and/or different lateral interactions in the interfacial film.

Another notable feature of the surface tension data in Fig. 1C is that for both the $C_{12}SO_4^-$ and $C_{14}SO_4^-$ systems, there is a local minimum that coincides with the highest viscoelasticity of the system.

**Table 1**

Equilibrium constants $K_{n1}$ and enthalpies $\Delta H_{n1}$ for the formation of α-CD:S ($n$ = 1) and (α-CD)$_2$:S ($n$ = 2) inclusion complexes for anionic surfactants (S) in $H_2O$, and for h-$C_{12}SO_4^-$ (fully protonated) and d-$C_{12}SO_4^-$ (fully deuterated) in $H_2O$ and $D_2O$.

| S (solvent) | $10^{-3}\, K_{11}$ ($M^{-1}$) | $10^{-3}\, K_{21}$ ($M^{-1}$) | $\Delta H_{11}$ (kJ mol$^{-1}$) | $\Delta H_{21}$ (kJ mol$^{-1}$) |
|---|---|---|---|---|
| | | $T$ = 283.15 K | | |
| $C_8SO_4^-$[a] | 9.5 ± 0.2 | 16.3 ± 0.3 | −27.6 ± 0.2 | −49.5 ± 0.4 |
| $C_{10}SO_4^-$[a] | 35.4 ± 0.5 | 23.9 ± 0.2 | −27.1 ± 0.1 | −53.9 ± 0.3 |
| $C_{12}SO_4^-$[a] | 61.1 ± 1.2 | 50.0 ± 0.8 | −22.8 ± 0.2 | −59.9 ± 0.4 |
| $C_{14}SO_4^-$ | 102.0 ± 3.3 | 82.6 ± 1.9 | −21.5 ± 0.3 | −58.8 ± 0.7 |
| $C_{12}SO_3^-$[a] | 62.4 ± 0.9 | 5.8 ± 0.1 | −22.9 ± 0.1 | −40.5 ± 0.3 |
| h/d-$C_{12}SO_4^-$ ($H_2O/D_2O$)[b] | 57.1 ± 0.4 | 57.2 ± 0.7 | −22.5 ± 0.1 | −61.2 ± 0.1 |
| | | $T$ = 293.15 K | | |
| $C_8SO_4^-$[a] | 6.2 ± 0.2 | 7.8 ± 0.1 | −31.4 ± 0.2 | −52.5 ± 0.3 |
| $C_{10}SO_4^-$[a] | 23.3 ± 0.3 | 10.7 ± 0.1 | −30.8 ± 0.1 | −57.7 ± 0.2 |
| $C_{12}SO_4^-$[a] | 42.4 ± 0.8 | 20.6 ± 0.3 | −27.8 ± 0.1 | −62.2 ± 0.3 |
| $C_{14}SO_4^-$ | 71.2 ± 2.3 | 34.7 ± 0.7 | −28.0 ± 0.2 | −61.0 ± 0.5 |
| $C_{12}SO_3^-$[a] | 43.2 ± 0.6 | 3.1 ± 0.1 | −28.1 ± 0.1 | −45.7 ± 0.3 |

[a] Values calculated from the temperature dependences of the equilibrium constants and enthalpies using the van't Hoff and Kichhoff equations, respectively, with parameters given in Ref. [32].

[b] Global fitting for {h-$C_{12}SO_4^-$ + $H_2O$}, {d-$C_{12}SO_4^-$ + $H_2O$}, {h-$C_{12}SO_4^-$ + $D_2O$} and {d-$C_{12}SO_4^-$ + $D_2O$} systems, performed using AFFINImeter [52].

Such a local minimum in the surface tension of mixtures has been observed previously in polyelectrolyte/surfactant mixtures, linked to a change in composition of the bulk species and the onset of precipitation through crossing a phase boundary [57]. In the present case, the increase in surface tension of around 5–6 mN/m that follows the local minimum for the $C_{12}SO_4^-$ system may be linked to the lower surface-activity of 1:1 complexes compared with 2:1 complexes, given the changes in the bulk composition obtained by ITC, although a direct interfacial characterization would be required to validate this inference.

### 3.2. Effects of temperature and total bulk concentration for {$C_{12}SO_4^-$ + α-CD} mixtures

Fig. 2A shows $E$ values for the {$C_{12}SO_4^-$ + α-CD} system at 283.15 and 293.15 K as a function of α-CD concentration. Here, the $r$ value was kept constant and equal to 0.340, i.e. the $r$ value where $E$ is a maximum at 283.15 K and [α-CD] = 10 mM (Fig. 1A). As $T$ is increased from 283.15 to 293.15 K, $E$ decreases markedly, showing that the film formation is very sensitive to temperature changes; in
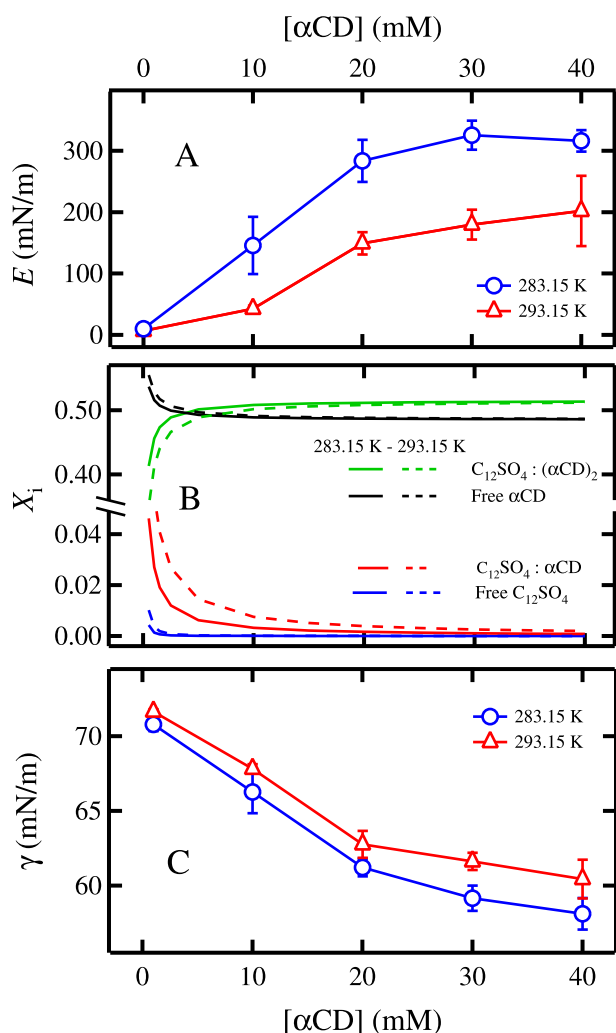
fact, at room temperature ($\cong$296.15 K) and [α-CD] = 10 mM $E$ is reduced to 30 mN/m, which is on the same order as the values obtained for the binary solutions {α-CD + water} and {$C_{12}SO_4^-$ + water} (9 mN/m and 6 mN/m, respectively). As the total amount of α-CD increases (keeping the same $r$ value), $E$ increases to very large values ($\cong$310 mN/m), leveling off at 30–40 mM of α-CD. In fact the magnitude of the viscoelasticity represents a 30-fold increase from the respective values for the binary solutions {α-CD + $H_2O$} and {$C_{12}SO_4^-$ + $H_2O$}. $E$ also strongly decreases as $T$ moves from 283.15 to 293.15 K for $C_{12}SO_3^-$ and $C_{14}SO_4^-$ at the surfactant concentration where $E$ is a maximum ($r$ = 0.200 and $r$ = 0.410, respectively, see Fig. 1A) and [α-CD] = 10 mM (see Part 9 of the Supplementary Material). In fact, the temperature dependence of $E$ in Fig. 2A occurs for all five surfactants at all $r$ values.

The corresponding distribution of species for $C_{12}SO_4^-$ at these two temperatures from ITC is shown in Fig. 2B with surface tension values in Fig. 2C. While the distribution of the species is almost the same (see Part 10 of the Supplementary Material), it is seen that $\gamma$(283.15 K) < $\gamma$(293.15 K), and that $\gamma$ decreases smoothly as the total amount of α-CD and $C_{12}SO_4^-$ increases (at constant $r$ = 0.340), reaching a value of approximately 60 mN/m. The higher viscoelasticity at 283.15 K may therefore be attributed to similar reasons as those describe above, namely a higher affinity of 2:1 complexes for the water/air interface (higher adsorbed amount) or stronger lateral interactions in the resulting interfacial layer.

The film response to temperature changes has been additionally examined using the same system with $r$ = 0.340, i.e. {3.4 mM $C_{12}SO_4^-$ + 10 mM α-CD}. The values of $\gamma$ as a function of time (after 90 min of equilibration time) was measured at 283.15 and 293.15 K, and switching back and forth from one temperature to the other. Fig. 3 shows that the film does not display hysteresis, i.e. in both 283.15 → 293.15 → 283.15 K and 293.15 → 283.15 → 293.15 K cycles the original $\gamma$ values are recovered. In other words, the film does not have any thermal memory and does not exist in a kinetically-trapped state. These data suggest that the film is in equilibrium with the bulk solution and supports the inference above that either there is a higher adsorbed amount at 283.15 K or the lateral intermolecular forces at the interface at this temperature are stronger.
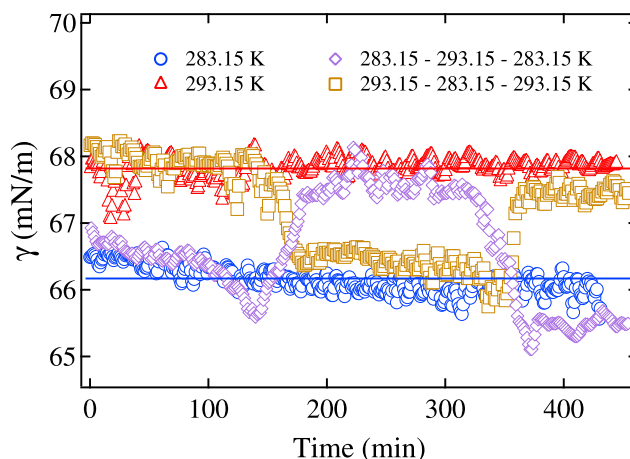


**Fig. 2.** (A) Dilatational modulus ($E$) for {$C_{12}SO_4^-$ + α-CD} mixtures at 283.15 K and 293.15 K as a function of α-CD concentration keeping $r$ = [surfactant]/[α-CD] constant at 0.340. In these experiments, the sinusoidal periodic oscillation was 0.20 Hz. The error bars are the standard deviations obtained from the measurements of three different drops. (B) Distribution of species in the bulk solution at 283.15 K and 293.15 K for {$C_{12}SO_4^-$ + α-CD} at $r$ = 0.340 calculated with AFFINImeter [52] with $K_{11}$ and $K_{21}$ from Table 1. (C) Corresponding surface tension values where the most dilute solutions correspond to 1 mM [α-CD].



**Fig. 3.** Surface tension ($\gamma$) as a function of time for the {3.4 mM $C_{12}SO_4^-$ + 10 mM α-CD} ($r$ = 0.340) system at 283.15 K (blue circles), 293.15 K (red triangles), for the cycles 283.15 → 293.15 → 283.15 K (purple diamonds) and 293.15 → 283.15 → 293.15 K (orange squares). The lines indicate the average surface tension values at 283.15 K (blue bottom line) and 293.15 K (red upper line). At times >400 min, upon returning to 283.15 and to 293.15 K, there are small deviations for $\gamma$. This is because at those times the pendant drop has lost 16% of its original volume, due to evaporation. (For interpretation of the references to colour in this figure legend, the reader is referred to the web version of this article.)

### 3.3. Interfacial adsorption of {$C_{12}SO_4^-$ + α-CD} mixtures

First we discuss data for {$C_{12}SO_4^-$ + α-CD} mixtures recorded at 283.15 K using ellipsometry, which is a technique sensitive to the adsorbed amount of material including contributions from any anisotropy (*i.e.* ordering of molecules) at the interface. Data shown in Fig. 4 were recorded for 1 h after surface formation for 6 samples at different *r* values; for reference, the bulk composition from ITC of these samples are reported in Table 2. It should be noted that it has been reported that α-CD monomers are not surface active [25–27] yet α-CD aggregates gather at the water/air interface over several hours with fluctuations in ellipsometry data resulting from the interfacial inhomogeneity evident from the outset [27]. The complexity of the present systems will become apparent in the following description and interpretation of the $\Delta_{surf}$ values in Fig. 4.

Sample a (*r* = 0.049) has initial fluctuations that can be attributed to the presence of macroscopic aggregates that float in and out of the laser beam. The ongoing lack of stability in the signal over the full hour suggests that the water/air interface continues to be populated by α-CD aggregates and is mobile as a result of its low viscoelasticity, as it has been observed by Brewster angle microscopy (BAM) and EP for a pure α-CD solution [27]. Sample b (*r* = 0.085) initially exhibits fluctuations but they extinguish suddenly as the signal stabilizes. The initial fluctuations can again be attributed to the presence of α-CD aggregates at the interface while stabilization of the signal can be attributed to the formation of a viscoelastic film due to the greater adsorption of 2:1 complexes. Sample c (*r* = 0.340) has an ellipsometry signal that is very high and stable from the outset, which is consistent with high viscoelasticity and low mobility of the interface (as observed previously by BAM [25]) resulting from the fast adsorption of 2:1 complexes to
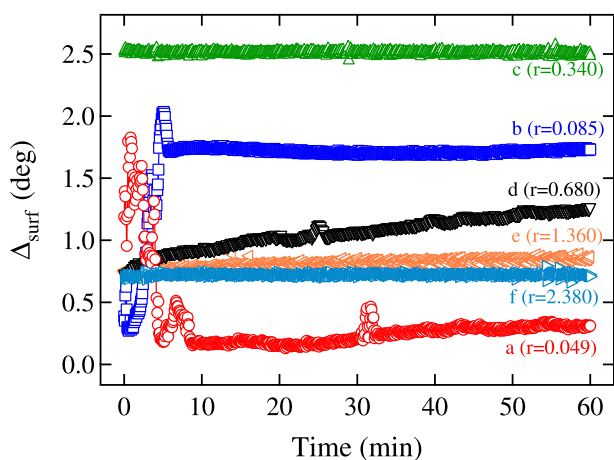
form a viscoelastic film. The magnitude of the phase shift is high compared with that of a surfactant monolayer recorded under the same conditions [72], which indicates that the film either has strong anisotropy as a result of a well ordered arrangement or is more extended than a monolayer. Sample d (*r* = 0.680) has a high ellipsometry signal from the outset but increases slowly with time and is not stable, which alludes to lateral inhomogeneities at the interface due to domains of α-CD/surfactant complexes and free surfactant. Sample e (*r* = 1.360) has intermediate behavior compared with samples d and f, which from these $\Delta_{surf}$ data alone seems unremarkable; however, as described below using NR, this sample exhibits an extreme behavior in the interfacial composition. Sample f (*r* = 2.380) has a constant ellipsometry signal that is similar to—but not the same—as that of a pure $C_{12}SO_4^-$ monolayer [72], which indicates extrapolation of the interfacial behavior towards that of a pure surfactant monolayer at high *r* values. In summary, ellipsometry has provided insight into the particular characteristics of the surface adsorbed material (quantity, homogeneity and order), which we have correlated with the species we know to be present in the bulk (Table 2). Nevertheless, the technique is not capable of giving us direct information about the composition of the films. For this reason, NR experiments were performed for the same system at 283.15 K.

We start with a first execution of NR that is highly sensitive to the interfacial composition. In this approach, the two scattering contributions from parallel measurements of a two-component mixture, one involving a given surface-active component in its hydrogenous form and another in its deuterated form, both recorded in ACMW solvent, are converted into the surface excess of the two components, assuming that the interfaces in the pair of measurements are chemically identical [57]. This approach is model-free and has been demonstrated to be much more accurate for the determination of the interfacial composition than the full structural execution of NR used traditionally [55].

Fig. 5A shows the scattering contribution from the NR data recorded over a broad range of *r* values at 283.15 K, where the 6 bulk compositions measured using EP are marked with arrows, and 6 samples were repeated. Two issues are apparent for the data at low *r* values. First, the reproducibility of sample is poor. Second, the condition is not met that the scattering contribution from {d-$C_{12}SO_4^-$ + α-CD} is higher than that of {h-$C_{12}SO_4^-$ + α-CD} (as the scattering length of d-$C_{12}SO_4^-$ is greater than that of h-$C_{12}SO_4^-$), which must be the case if each pair of samples were chemically identical. These features suggest variability from sample to sample of the interfacial films created. It can be inferred that the time-dependent adsorption of α-CD aggregates, as suggested from the EP analysis above (Fig. 4), indeed dominates these samples. The reproducibility of the other samples is excellent, and the condition that the scattering contribution of {d-$C_{12}SO_4^-$ + α-CD} exceeds that of {h-$C_{12}SO_4^-$ + α-CD} is met. As such, the standard approach to calculate the interfacial composition using this technique [57] was performed for all the samples to the right of the vertical dotted line in Fig. 5A, the results being shown in Fig. 5B.

In Fig. 5A, for 0.085 < *r* < 0.340 (*i.e.* between b and c), the samples that exhibit very high viscoelasticity (Fig. 1A), the surface

**Fig. 4.** Kinetic evolution of the ellipsometry phase shift ($\Delta_{surf}$) for the {$C_{12}SO_4^-$ + 10 mM α-CD} system at 283.15 K for six different concentration ratio *r* = [surfactant]/[α-CD], where *r* = (a) 0.049, (b) 0.085, (c) 0.340, (d) 0.680, (e) 1.360, and (f) 2.380.

**Table 2**
Values for the distribution of species obtained from ITC measurements at 283.15 K in the bulk solution (%) for the {$C_{12}SO_4^-$ + 10 mM α-CD} system for several *r* values.

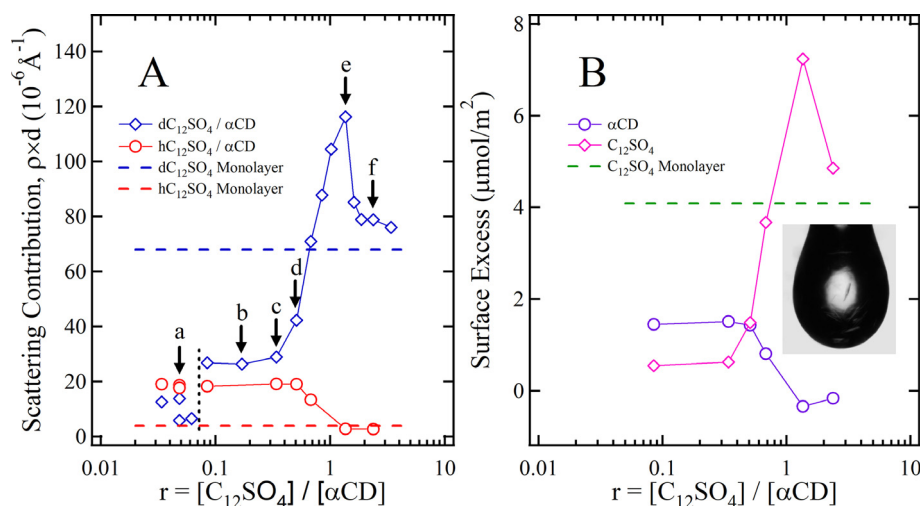| | $r = [C_{12}SO_4^-]/[α-CD]$ | | | | | |
| --- | --- | --- | --- | --- | --- | --- |
| | a<br>0.049 | b<br>0.085 | c<br>0.340 | d<br>0.680 | e<br>1.360 | f<br>2.380 |
| 2:1 complexes (%) | 5.20 | 9.39 | 50.88 | 58.29 | 20.05 | 8.12 |
| 1:1 complexes (%) | 0.01 | 0.02 | 0.32 | 29.16 | 33.63 | 25.61 |
| Free surfactant (%) | 0.00 | 0.00 | 0.00 | 11.96 | 46.23 | 66.24 |
| Free α-CD (%) | 94.79 | 90.59 | 48.80 | 0.59 | 0.09 | 0.03 |

**Fig. 5.** (A) Scattering contributions in the low-$q$ analysis method of NR for the {$C_{12}SO_4^-$ + 10 mM $\alpha$-CD} system at 283.15 K for different values of $r$ = [surfactant]/[$\alpha$-CD], where labels a–f correspond to the same samples measured using ellipsometry (Fig. 4 and Table 2); red and blue horizontal dashed lines mark the respective scattering contributions for a full monolayer of h-$C_{12}SO_4^-$ and d-$C_{12}SO_4^-$; vertical black dotted line marks the division between low $r$ values where the data are not reproducible and high $r$ values where they are reproducible. The repeated samples are $r$ = 0.049, 0.085 and 2.380 for samples with h-$C_{12}SO_4^-$, and $r$ = 0.049, 0.085 and 0.340 for samples with d-$C_{12}SO_4^-$. (B) Resulting surface excesses from analysis of the data in panel A using the methodology described in ref. [57]; horizontal dashed line marks the value for a full $C_{12}SO_4^-$ monolayer. The inset is a photograph of a hanging droplet of sample e where micro-crystals at the water/air interface can be observed.

excesses of $\alpha$-CD and surfactant ($\Gamma_{\alpha\text{-CD}}$ and $\Gamma_{\text{surfactant}}$, respectively) are approximately constant, and the interfacial stoichiometry of $\Gamma_{\alpha\text{-CD}}/\Gamma_{\text{surfactant}}$ with increasing $r$ falls slightly from 2.6:1 to 2.4:1. These data provide strong evidence that the interface is populated by 2:1 complexes along with some residual $\alpha$-CD aggregates. The facts that the interfacial composition changes only slightly from $r$ = 0.085 to 0.340, yet the EP signal increases markedly, indicate that a reduction in the number of $\alpha$-CD aggregates in the film results in a strong increase in the order of the layer of 2:1 complexes. With increasing $r$ values to 1.360 (*i.e.* between d to e), the surface excess of $C_{12}SO_4^-$ exceeds that of a single monolayer while the amount of $\alpha$-CD at the interface falls to around zero; the slightly negative values hint that sample-dependent variability in parallel measurements again creep into play. While the large amount of surfactant at the interface may be initially surprising, a photograph of a hanging droplet shown in the inset to Fig. 5B reveals the presence of micro-crystals at the water/air interface. This observation can be attributed to the fact that the Krafft point of $C_{12}SO_4^-$ coincides with the measurement temperature of 283.15 K [73], *i.e.*, as $C_{12}SO_4^-$ molecules augment in the bulk with increasing $r$, the free surfactant crystallizes, and the resulting crystals abruptly disrupt the viscoelasticity when they contact the interfacial film. It follows that the viscoelasticity diminishes more gradually for the {$C_{14}SO_4^-$ + $\alpha$-CD} system as the Krafft temperature of $C_{14}SO_4^-$ is higher and hence the gradual build-up of free surfactant in the bulk is required for domains of surfactant to compete with the adsorbed complexes at the interface. From the experimental data, it is not clear whether the adsorption of 1:1 complexes—which are present in the bulk—also contribute to a reduction in the viscoelasticity of the films with increasing $r$ values, if indeed they are surface-active. Even so, indirect evidence in the form of bulk MD simulations has shown that a locally high concentration of 1:1 can spontaneously form 2:1 complexes (see Part 11 of the Supplementary Material). Additional experimental data or direct simulations at the water/air interface, however, would be required to elaborate on this point. At the highest $r$ value of 2.380 (*i.e.* sample f), the surface excess of $C_{12}SO_4^-$ reduces and is close to that of a saturated monolayer while that of $\alpha$-CD remains minimal. That the measured surface excess of $C_{12}SO_4^-$ does not match exactly that of a saturated monolayer is consistent with the observation from EP (Fig. 4).

In summary, our comprehensive interfacial adsorption characterization has shown that the high viscoelasticity of the {$C_{12}SO_4^-$ + $\alpha$-CD} system at 283.15 K results when a highly ordered layer of 2:1 complexes has the lowest amount of any other components at the interface. As $r$ decreases from its optimum value of 0.340 the number of $\alpha$-CD aggregates at the interface increases, and as $r$ increases monolayer domains or microcrystals of $C_{12}SO_4^-$ gather at the interface. Both effects result in a reduction of the viscoelasticity. We now turn to the structure of the highly viscoelastic films in order to resolve whether they consist of a monolayer of 2:1 complexes or a more extended structure, and to discuss their physical basis.

### 3.4. Interfacial structure of {$C_{12}SO_4^-$ + $\alpha$-CD} mixtures

In order to resolve the structure of the interfacial layers produced for the {$C_{12}SO_4^-$ + $\alpha$-CD} system at 283.15 K, and in particular to gain insight into the underlying nature of the viscoelastic vs. non-viscoelastic films, a second execution of NR involving data recorded over the fully accessible $q$-range in 4 isotopic contrasts was performed for 4 samples with the $r$ values 0.085 (A), 0.340 (B), 0.510 (C) and 1.360 (D). Considering the relation between the dilatational modulus and the bulk distribution of species discussed above, we employed a model to fit the data that involves a single homogenous layer comprising 2:1 complexes, water and the predominant free bulk species: $\alpha$-CD for samples A and B, and $C_{12}SO_4^-$ for samples C and D; note that models involving the adsorption of 1:1 complexes were also considered but they did not improve the quality of the fits.

To place into context the following observations, it is important first to appreciate the shape and dimensions of the building blocks of the highly viscoelastic films, *i.e.*, the 2:1 complexes. From MD simulations using nucleus–nucleus distances (for comparison with neutron scattering data) Fig. 6 shows that the complexes are cylindrical-shaped with a maximum height (along the $C_{12}SO_4^-$ axis) of 16.1 Å and a maximum diameter (of the $\alpha$-CD rings) of 13.2 Å. Additionally, we recall that in pure $\alpha$-CD solutions, aggregates adsorb to the water/air interface to produce a layer with a fitted thickness of 40 Å [27].

Fig. 7 shows the measured NR data and model fits where it is clear that the employed homogenous single-layer model is capable
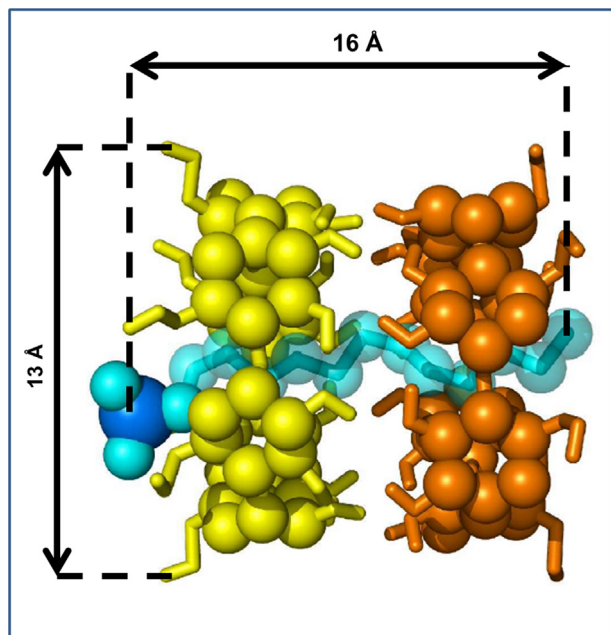
**Fig. 6.** Snapshot of a $(\alpha\text{-CD})_2:C_{12}SO_4^-$ complex taken from an equilibrated MD simulation in aqueous solution. The dimensions of the cylindrical-shaped structure are indicated.

**Table 3**
Component proportions and thickness of a model of a single homogenous layer obtained from the fitting of the NR data for the $\{C_{12}SO_4^- + 10\ mM\ \alpha\text{-CD}\}$ system at 283.15 K.

| | $r = [C_{12}SO_4^-]/[\alpha\text{-CD}]$ | | | |
| --- | --- | --- | --- | --- |
| | 0.085 | 0.340 | 0.510 | 1.360 |
| 2:1 complexes (%) | 44 | 69 | 54 | 0 |
| Free α-CD (%) | 19 | 7 | – | – |
| Free surfactant (%) | – | – | 46 | 100 |
| Water (%) | 37 | 24 | 0 | 0 |
| Thickness (nm) | 1.70 | 1.50 | 0.94 | 1.70 |

reflectivity were taken from independent fittings of pure $D_2O$. The obtained values for the fitted parameters, together with the remaining proportion of water in the layer, are reported in Table 3. The composition of the interface at different $r$ values is consistent with results from the low-$q$ analysis described above, so the new information comes in the thickness and hydration of the layers.

For the viscoelastic films produced from the samples with the lower two $r$ values (samples A and B), the layers have a thickness of 15–17 Å and a hydration of 24–37%. Immediately, it can be concluded that the 2:1 complexes at the interface are present as a monolayer rather than in an extended structure. As a heterogeneous layer model with patches of α-CD aggregates did not improve the quality of the fits, it can be assumed that the α-CD aggregates are present at the interface on a length scale that is smaller than the coherence length of the measurements (~ 10–100 μm) [60]. In this case, the thickness contribution to the layer will be averaged by area fraction of the species. As such, if it were assumed that the α-CD aggregates again have a thickness of around 40 Å, it would place the thickness contribution of the 2:1 complexes as 12–13 Å, *i.e.*, closer to its smaller axis (Fig. 6).
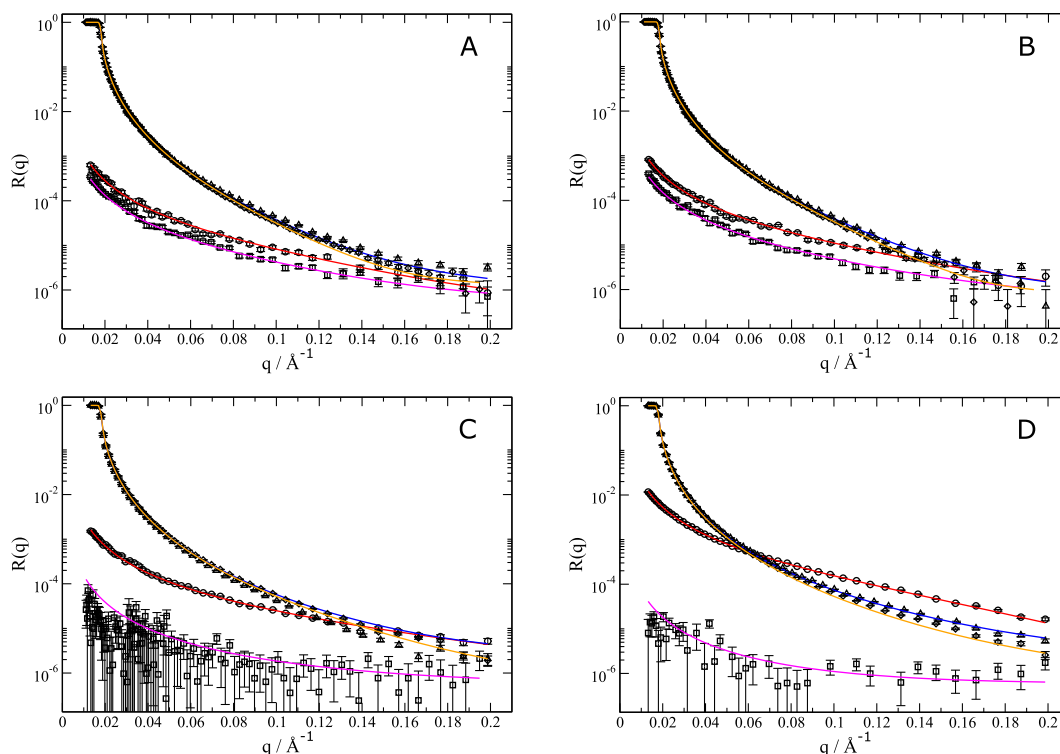
of fitting data recorded in the 4 isotopic contrasts for each of 4 measured $r$ values using just 3 parameters: the layer thickness, and the proportions of the 2:1 complexes and free species (α-CD or $C_{12}SO_4^-$). The roughness of both interfaces was fixed to 3 Å while the scattering length density of the solvent and the background



**Fig. 7.** Experimental neutron reflectivity data (symbols) and model fits (lines) obtained using a homogenous single-layer model in 4 different isotopic contrasts: $\{d\text{-}C_{12}SO_4^- + \alpha\text{-CD}\}$ in ACMW (circles + red), $\{d\text{-}C_{12}SO_4^- + \alpha\text{-CD}\}$ in $D_2O$ (triangles + blue), $\{h\text{-}C_{12}SO_4^- + \alpha\text{-CD}\}$ in ACMW (squares + pink) and $\{h\text{-}C_{12}SO_4^- + \alpha\text{-CD}\}$ in $D_2O$ (diamonds + orange). The data were measured at 283.15 K with $r = [C_{12}SO_4^-]/[\alpha\text{-CD}]$: 0.085 (A), 0.340 (B) and 0.510 (C) and 1.360 (D) with [α-CD] = 10 mM. (For interpretation of the references to colour in this figure legend, the reader is referred to the web version of this article.)

Nevertheless, it should be underlined that given the small difference between the longer and shorter axes of the complexes, this result represents only a hint rather than firm evidence of the orientation of the 2:1 complexes with the surfactant chains parallel to the interface.

Previous MD simulations performed using the GROMOS force field [37] also suggested that the 2:1 complexes are oriented with the surfactant chains parallel to the water/air interface but, based on the available experimental data, we cannot discard that the films are formed by complexes orientated with the chains in a perpendicular orientation. Both scenarios can be explained in terms of intermolecular interactions as follows. *Parallel orientation:* MD simulations indicate that the 2:1 complexes are extremely tight, with an average of ~9.5 H-bonds between both CDs out of a maximum of 12 [37]. Such a belt of H-bonds between both CDs is expected to induce a high orientation of surrounding water molecules. The release of many of these molecules upon adsorption with the surfactant chains parallel to the interface should be entropically favourable. This factor would explain not only the adsorption of a single complex unit but also the interaction between contiguous complexes. Additionally, the charge of the $C_{12}SO_4^-$ head group induces a high dipolar moment for the 2:1 complex, which is reduced when an equivalent unit joins to the surface in an antiparallel orientation with respect to the contiguous complex. These two interactions may favour the formation of highly ordered monolayers, as observed experimentally in the present work. Such films require a high concentration of counterions very close to the interface to compensate the high charge density of the 2:1 complexes monolayer. These counterions could be responsible for preventing the vertical growth of the film to form more extended layers, as have been observed using atomic force microscopy following deposition of $\{C_{12}SO_4^- + \alpha\text{-CD}\}$ films on mica [25]. *Perpendicular orientation:* In this scenario, the adsorption of individual complexes would not release the ordered water molecules around the OH belt joining both CDs, but the two-dimensional aggregation of many complexes would do. Another important difference with respect to the parallel orientation is that all the complexes would probably be oriented with the surfactant head groups pointing toward the water bulk, so the dipolar interaction coming from the relative orientation of contiguous complexes would be unfavourable due to the stabilization of the monolayer. The latter interaction would not be critical since monolayers of amphiphiles (including $C_{12}SO_4^-$) are stable at the interface, but it is clearly a destabilizing contribution for two-dimensional aggregation.

For the non-viscoelastic films at the higher two *r* values (samples C and D), the model fits converge to zero hydration in both cases, which demonstrates the compactness of the films. This result implies that the high water content associated in samples A and B are linked to the presence of α-CD aggregates rather than the 2:1 complexes. For sample C ($r = 0.510$), the layer is <1 nm thick, and is consistent with a co-existence of complexes and free surfactant at the interface. It is not evident from the NR data whether such an interfacial arrangement consists of a homogenous layer or a heterogeneous layer with phase separation between domains. Nevertheless, we know that this film exhibits a sharp reduction in the viscoelasticity, which shows that the presence of free surfactant at the interface reduces the viscoelasticity of the monolayers. For sample D ($r = 1.360$), the layer fits to an extended layer of pure $C_{12}SO_4^-$. As discussed above, an average thickness that exceeds a monolayer for this sample can be attributed to the presence of micro-crystals of $C_{12}SO_4^-$ at the interface due to the measurement being performed at a temperature equal to the Krafft point of the surfactant.

In summary, the highest viscoelasticity corresponds to a monolayer of highly ordered 2:1 complexes with the minimum amount of any other component (e.g. hydrated α-CD aggregates or free surfactant). An indirect indication from NR as well as previous results from MD simulations suggest that the orientation of the 2:1 complexes in the films is with the surfactant chains parallel to the water/air interface, and we have rationalized the driving forces for adsorption in this case. Nevertheless, additional direct experimental evidence would be required for conclusive proof of this inference.

## 4. Conclusions

We have shown that films formed at the water/air interface from aqueous solutions of α-CD and the sodium salts of *n*-alkyl sulfate or sulfonate surfactants possess remarkable viscoelasticity. A combination of measurements using surface dilational rheology, isothermal titration calorimetry, surface tensiometry, ellipsometry and neutron reflectometry as well as molecular dynamics simulations have led to a comprehensive characterization of these systems.

The viscoelasticity of the films can be tuned through changes in *(i)* bulk composition, *(ii)* temperature, *(iii)* alkyl chain length and *(iv)* head group type, and the property can even be set to a given desired value (or range of values), clearly showing the versatility of CD-based systems when complexed to anionic surfactants. It was found that the response of the film to mechanical perturbations is strongly linked to the distribution of species in the bulk solution and, in particular, to high concentrations of (α-CD)$_2$:surfactant inclusion complexes. Other important factors connected to the high viscoelasticity values can be the affinity of 2:1 complexes for the water/air interface and/or the strength of lateral interactions in the resulting interfacial film.

2:1 complexes have been previously reported as building blocks of many different structures that have interesting properties. Using linear oils as guest molecules, Mathapa and Paunov published a series of articles aimed at understanding the self-assembly of such complexes at water/air and water/oil interfaces [74,75]. Their optical and scanning electron microscopy images clearly show how the inclusion complexes are adsorbed to polar-nonpolar interfaces in a parallel orientation. These systems and the experiments are closely connected to our results performed at the water/air interface using anionic surfactants. In another series of reports, this time employing anionic surfactants, Jiang et al. and Yang et al. studied the structure of (β-CD)$_2$:$C_{12}SO_4^-$ complexes at different bulk concentrations [76–78]. They observed interesting patterns, including compartmentalization in giant capsids. They proposed the formation of bilayers of 2:1 complexes where each leaflet would consist of parallel 2:1 complexes interacting through H-bonds and the two leaflets would be faced by the tail side of the complexes, with the $C_{12}SO_4^-$ head exposed to the solvent on both sides of the bilayer. The affinity of α-CD for $C_{12}SO_4^-$, as well as its higher ability to form 2:1 complexes as compared to β-CD, stimulated us to focus on the complexes formed by the same type of surfactants with the smaller cavity volume α-CD in the present work.

In order to gain additional insight into the viscoelastic nature of the films, we applied a combination of ellipsometry and neutron reflectometry to mixtures of α-CD and sodium dodecylsulfate at 283.15 K over a broad range of bulk compositions. The marked complexity of the system became apparent. The most viscoelastic films were shown to consist of a highly ordered monolayer of 2:1 complexes with a minimum amount of hydrated α-CD aggregates or free surfactant from the bulk embedded in them. With decreasing surfactant concentration, the viscoelasticity is reduced as the amount of hydrated α-CD aggregates in the film increases and the amount of 2:1 complexes decreases. With increasing bulk surfactant concentration, the viscoelasticity is reduced abruptly due to the adsorption of free

surfactant and penetration in the film of surfactant crystals, which are present in the bulk as the measurement temperature coincides with the Krafft point of the surfactant.

The physical origin of the highly viscoelastic behavior has been discussed. Previously an indication from molecular dynamics simulations suggested that the complexes align with the surfactant chains parallel to the interface. The orientation of the inclusion complexes at the surface of cyclodextrinosomes, observed by different microscopy methods, also support this result [74,75,79–81]. In the present work, there is an experimental indication to this effect from neutron reflectometry. However, this inference can be considered only tentative given the small difference in the dimensions of the complexes parallel and perpendicular to the surfactant axis. Nevertheless, we described the possible driving forces for adsorption of the complexes both in this configuration and with the surfactant chains perpendicular to the interface. In the former case, reasons can be related to the entropy gain associated from the release of highly ordered water molecules in a belt around the outer $\alpha$-CD surface, and electrostatic dipolar interactions due to the antiparallel arrangement of contiguous complexes. The same driving forces might explain other similar self-assembly patterns [74–81].

The strong dependence of the viscoelasticity on several experimental parameters that are easy to control might be useful in the design of functional films with a specific response to mechanical perturbations for practical applications. However, several questions remain open in order to understand better the molecular interactions. For instance, the specific orientation of the 2:1 complexes at the interface has not been conclusively resolved, although our results, and the extrapolation of results previously observed for similar systems, point to a preference for the parallel orientation. Conclusive information on the orientation of the complexes could be achieved possibly using vibrational sum-frequency generation spectroscopy. Moreover, the reasons why the studied systems lead to a film consisting of a single monolayer of complexes rather than a more extended film are not clear. Additional simulations using molecular dynamics to determine the counterion distribution associated with the films may help in this regard. Other avenues for future work are studies of the behavior of mixed surfactant solutions, where the competition of different inclusion complexes in the films could be studied using neutron reflectometry. Also, further work on the effects of the surfactant head group could lead to information about why various systems are more viscoelastic than others.

There is broad scope in the future for a detailed characterization at the molecular level of highly viscoelastic films consisting of 2:1 inclusion complexes made from $\alpha$-CD and anionic surfactants using a combination of experimental and computational tools. The tunable nature of the films depends on the specific molecule threaded by the cyclodextrins, on the employed solvent and on specific chemical substitutions for the cyclodextrins. Potential applications can be related to new functional materials with specific mechanical, electrical, chemical, thermal, optical or even magnetic properties to filters, coatings, molecular sensors and means to catalyze specific chemical reactions. Some of these applications based on cyclodextrin complexes have already been explored [74,81–84] but our work shows clearly that there is high scope for the development of new devices, materials and applications based on these apparently simple molecules.

## Declaration of Competing Interest

The authors declare that they have no known competing financial interests or personal relationships that could have appeared to influence the work reported in this paper.

## Appendix A. Supplementary material

Supplementary data to this article can be found online at https://doi.org/10.1016/j.jcis.2019.12.012.

## References

[1] M.V. Rekharsky, Y. Inoue, Complexation thermodynamics of cyclodextrins, Chem. Rev. 98 (1998) 1875–1918, https://doi.org/10.1021/cr970015o.
[2] H. Dodziuk, Rigidity versus flexibility. A review of experimental and theoretical studies pertaining to the cyclodextrin nonrigidity, J. Mol. Struct. 614 (2002) 33–45, https://doi.org/10.1016/S0022-2860(02)00236-3.
[3] E. Mixcoha, J. Campos-Terán, Á. Piñeiro, Surface adsorption and bulk aggregation of cyclodextrins by computational molecular dynamics simulations as a function of temperature: $\alpha$-CD vs $\beta$-CD, J. Phys. Chem. B 118 (2014) 6999–7011, https://doi.org/10.1021/jp412533b.
[4] A.J.M. Valente, O. Söderman, The formation of host-guest complexes between surfactants and cyclodextrins, Adv. Colloid Interface Sci. 205 (2014) 156–176, https://doi.org/10.1016/j.cis.2013.08.001.
[5] A. Hashidzume, A. Harada, Recognition of polymer side chains by cyclodextrins, Polym. Chem. 2 (2011) 2146–2154, https://doi.org/10.1039/c1py00162k.
[6] T. Loftsson, D. Duchêne, Cyclodextrins and their pharmaceutical applications, Int. J. Pharm. 329 (2007) 1–11, https://doi.org/10.1016/j.ijpharm.2006.10.044.
[7] A. Ikeda, R. Funada, K. Sugikawa, Different stabilities of liposomes containing saturated and unsaturated lipids toward the addition of cyclodextrins, Org. Biomol. Chem. 14 (2016) 5065–5072, https://doi.org/10.1039/c6ob00535g.
[8] G. Wenz, B. Han, A. Mu, Cyclodextrin rotaxanes and polyrotaxanes, Chem. Rev. 106 (2006) 782–817, https://doi.org/10.1021/cr970027.
[9] A. Cooper, Effect of cyclodextrins on the thermal stability of globular proteins, J. Am. Chem. Soc. 114 (1992) 9208–9209, https://doi.org/10.1021/ja00049a074.
[10] http://ep.espacenet.com, (n.d.).
[11] G. Chen, M. Jiang, Cyclodextrin-based inclusion complexation bridging supramolecular chemistry and macromolecular self-assembly, Chem. Soc. Rev. 40 (2011) 2254–2266, https://doi.org/10.1039/c0cs00153h.
[12] A. Harada, Y. Takashima, M. Nakahata, Supramolecular polymeric materials via cyclodextrin-guest interactions, Acc. Chem. Res. 47 (2014) 2128–2140, https://doi.org/10.1021/ar500109h.
[13] J.H.T. Luong, R.S. Brown, K.B. Male, M.V. Cattaneo, S. Zhao, Enzyme reactions in the presence of cyclodextrins: biosensors and enzyme assays, Trends Biotechnol. 13 (1995) 457–463, https://doi.org/10.1016/S0167-7799(00)89002-2.
[14] T. Ogoshi, A. Harada, Chemical sensors based on cyclodextrin derivatives, Sensors 8 (2008) 4961–4982, https://doi.org/10.3390/s8084961.
[15] A. Wang, W. Shi, J. Huang, Y. Yan, Adaptive soft molecular self-assemblies, Soft Matter. 12 (2016) 337–357, https://doi.org/10.1039/c5sm02397a.

[16] R. Challa, A. Ahuja, J. Ali, R.K. Khar, Cyclodextrins in drug delivery: an updated review, AAPS PharmSciTech. 6 (2005) 329–357, https://doi.org/10.1517/17425247.2.1.335.

[17] L. Xiao, Y. Ling, A. Alsbaiee, C. Li, D.E. Helbling, W.R. Dichtel, β-cyclodextrin polymer network sequesters perfluorooctanoic acid at environmentally relevant concentrations, J. Am. Chem. Soc. 139 (2017) 7689–7692, https://doi.org/10.1021/jacs.7b02381.

[18] L.F. Villalobos, T. Huang, K.V. Peinemann, Cyclodextrin films with fast solvent transport and shape-selective permeability, Adv. Mater. 29 (2017) 1–7, https://doi.org/10.1002/adma.201606641.

[19] W. Li, G. Jin, H. Chen, J. Kong, Highly sensitive and reproducible cyclodextrin-modified gold electrodes for probing trace lead in blood, Talanta. 78 (2009) 717–722, https://doi.org/10.1016/j.talanta.2008.12.030.

[20] A.W. Coleman, I. Nicolis, N. Keller, J.P. Dalbiez, Aggregation of cyclodextrins: an explanation of the abnormal solubility of β-cyclodextrin, J. Incl. Phenom. Mol. Recognit. Chem. 13 (1992) 139–143, https://doi.org/10.1007/BF01053637.

[21] G. Gonzalez-Gaitano, P. Rodriguez, J.R. Isasi, M. Fuentes, G. Tardajos, M. Sanchez, The aggregation of cyclodextrins as studied by photon correlation spectroscopy, J. Incl. Phenom. Macrocycl. Chem. 44 (2002) 101–105, https://doi.org/10.1023/A:1023065823358.

[22] I. Puskás, M. Schrott, M. Malanga, L. Szente, Characterization and control of the aggregation behavior of cyclodextrins, J. Incl. Phenom. Macrocycl. Chem. 75 (2013) 269–276, https://doi.org/10.1007/s10847-012-0127-7.

[23] M. Messner, S.V. Kurkov, R. Flavià-Piera, M.E. Brewster, T. Loftsson, Self-assembly of cyclodextrins: the effect of the guest molecule, Int. J. Pharm. 408 (2011) 235–247, https://doi.org/10.1016/j.ijpharm.2011.02.008.

[24] Y. He, P. Fu, X. Shen, H. Gao, Cyclodextrin-based aggregates and characterization by microscopy, Micron. 39 (2008) 495–516, https://doi.org/10.1016/j.micron.2007.06.017.

[25] J. Hernández-Pascacio, C. Garza, X. Banquy, N. Díaz-Vergara, A. Amigo, S. Ramos, R. Castillo, M. Costas, Á. Piñeiro, Cyclodextrin-based self-assembled nanotubes at the water/air interface, J. Phys. Chem. B 111 (2007) 12625–12630, https://doi.org/10.1021/jp076576t.

[26] J. Hernández-Pascacio, X. Banquy, S. Pérez-Casas, M. Costas, A. Amigo, Á. Piñeiro, A small molecular size system giving unexpected surface effects: α-cyclodextrin + sodium dodecylsulfate in water, J. Colloid Interface Sci. 328 (2008) 391–395, https://doi.org/10.1016/j.jcis.2008.09.002.

[27] J. Hernandez-Pascacio, Á. Piñeiro, J.M. Ruso, N. Hassan, R.A. Campbell, J. Campos-Terán, M. Costas, Complex behavior of aqueous α-cyclodextrin solutions. Interfacial morphologies resulting from bulk aggregation, Langmuir 32 (2016) 6682–6690, https://doi.org/10.1021/acs.langmuir.6b01646.

[28] L. Jiang, Y. Yan, J. Huang, Versatility of cyclodextrins in self-assembly systems of amphiphiles, Adv. Colloid Interface Sci. 169 (2011) 13–25, https://doi.org/10.1016/j.cis.2011.07.002.

[29] M. Ferreira, H. Bricout, N. Azaroual, D. Landy, S. Tilloy, F. Hapiot, E. Monflier, Cyclodextrin/amphiphilic phosphane mixed systems and their applications in aqueous organometallic catalysis, Adv. Synth. Catal. 354 (2012) 1337–1346, https://doi.org/10.1002/adsc.201100837.

[30] H. Dodziuk, Cyclodextrins and Their Complexes: Chemistry, Analytical Methods, Applications, Wiley, 2006, https://doi.org/10.1002/3527608982.

[31] P. Brocos, X. Banquy, N. Díaz-Vergara, S. Pérez-Casas, Á. Piñeiro, M. Costas, A critical approach to the thermodynamic characterization of inclusion complexes: multiple-temperature isothermal titration calorimetric studies of native cyclodextrins with sodium dodecylsulfate, J. Phys. Chem. B 115 (2011) 14381–14396, https://doi.org/10.1021/jp208740b.

[32] D. Ondo, M. Costas, Complexation thermodynamics of α-cyclodextrin with ionic surfactants in water, J. Colloid Interface Sci. 505 (2017) 445–453, https://doi.org/10.1016/j.jcis.2017.05.093.

[33] S. Ishikawa, S. Hirota, S. Neya, N. Funasaki, Molecular motions of alpha-cyclodextrin on a dodecyl chain studied by molecular dynamics simulations, Chem. Pharm. Bull. (Tokyo) 54 (2006) 528–534, https://doi.org/10.1248/cpb.54.528.

[34] R. Semino, J. Rodríguez, Molecular dynamics study of ionic liquids complexation within β-cyclodextrins, J. Phys. Chem. B 119 (2015) 4865–4872, https://doi.org/10.1021/acs.jpcb.5b00909.

[35] W. Khuntawee, P. Wolschann, T. Rungrotmongkol, J. Wong-Ekkabut, S. Hannongbua, Molecular dynamics simulations of the interaction of beta cyclodextrin with a lipid bilayer, J. Chem. Inf. Model. 55 (2015) 1894–1902, https://doi.org/10.1021/acs.jcim.5b00152.

[36] Á. Piñeiro, X. Banquy, S. Pérez-Casas, E. Tovar, A. García, A. Villa, A. Amigo, A.E. Mark, M. Costas, On the characterization of host-guest complexes: surface tension, calorimetry, and molecular dynamics, of cyclodextrins with a non-ionic surfactant, J. Phys. Chem. B 111 (2007) 4383–4392, https://doi.org/10.1021/jp0688815.

[37] P. Brocos, N. Díaz-Vergara, X. Banquy, S. Pérez-Casas, M. Costas, Á. Piñeiro, Similarities and differences between cyclodextrin-sodium dodecylsulfate host-guest complexes of different stoichiometries: molecular dynamics simulations at several temperatures, J. Phys. Chem. B 114 (2010) 12455–12467, https://doi.org/10.1021/jp103223u.

[38] J. Pelipenko, J. Kristl, R. Rošic, S. Baumgartner, P. Kocbek, Interfacial rheology: an overview of measuring techniques and its role in dispersions and electrospinning, Acta Pharm. 62 (2012) 123–140, https://doi.org/10.2478/v10007-012-0018-x.

[39] V.N. Nazakov, V.M. Knyazevich, O.V. Sinyachenko, V.B. Fainerman, R. Miller, Interfacial rheology, in: R. Miller, L. Liggieri (Eds.), Prog. Colloids Interface Sci.,

[40] S. Mielke, W. Abuillan, M. Veschgini, X. Liu, O. Konovalov, M.P. Krafft, M. Tanaka, Influence of perfluorohexane-enriched atmosphere on viscoelasticity and structural order of self-assembled semifluorinated alkanes at the air-water interface, ChemPhysChem 1698–1705 (2019), https://doi.org/10.1002/cphc.201900316.

[41] A. Kovalenko, P. Polavarapu, J.L. Gallani, G. Pourroy, G. Waton, M.P. Krafft, Super-elastic air/water interfacial films self-assembled from soluble surfactants, ChemPhysChem 15 (2014) 2440–2444, https://doi.org/10.1002/cphc.201402248.

[42] D. Kowalczyk, W. Gustaw, M. Świeca, B. Baraniak, A study on the mechanical properties of pea protein isolate films, J. Food Process. Preserv. 38 (2014) 1726–1736, https://doi.org/10.1111/jfpp.12135.

[43] L. Zhang, H.Q. Sun, L. Zhang, Z.Q. Li, L. Luo, S. Zhao, Interfacial dilational rheology related to enhance oil recovery, Soft Matter. 7 (2011) 7601–7611, https://doi.org/10.1039/c1sm05234a.

[44] H. Xing, H.T. Zhou, H.Q. Yu, Z.M. Gou, J.X. Xiao, Participation of inclusion complexes in the surface adsorbed layer in mixtures of α-cyclodextrin and cationic-anionic hydrogenated and fluorinated surfactants: a surface tension proof, J. Chem. Eng. Data. 56 (2011) 1423–1432, https://doi.org/10.1021/je101149h.

[45] Y. Bai, G.Y. Xu, X. Xin, H.Y. Sun, H.X. Zhang, A.Y. Hao, X.D. Yang, L. Yao, Interaction between cetyltrimethylammonium bromide and β-cyclodextrin: surface tension and interfacial dilational viscoelasticity studies, Colloid Polym. Sci. 286 (2008) 1475–1484, https://doi.org/10.1007/s00396-008-1918-7.

[46] I. Kuzmenko, H. Rapaport, K. Kjaer, J. Als-Nielsen, I. Weissbuch, M. Lahav, L. Leiserowitz, Design and characterization of crystalline thin film architectures at the air-liquid interface: simplicity to complexity, Chem. Rev. 101 (2001) 1659–1696, https://doi.org/10.1021/cr990038y.

[47] I. Varga, R. Mészáros, T. Gilányi, Adsorption of sodium alkyl sulfate homologues at the air/solution interface, J. Phys. Chem. B 111 (2007) 7160–7168, https://doi.org/10.1021/jp071344f.

[48] D.J. Jobe, V.C. Reinsborough, S.D. Wetmore, Sodium dodecylsulfate micellar aggregation numbers in the presence of cyclodextrins, Langmuir 11 (1995) 2476–2479, https://doi.org/10.1021/la00007a027.

[49] R.A. Campbell, M. Yanez Arteta, A. Angus-Smyth, T. Nylander, I. Varga, Multilayers at interfaces of an oppositely charged polyelectrolyte/surfactant system resulting from the transport of bulk aggregates under gravity, J. Phys. Chem. B 116 (2012) 7981–7990, https://doi.org/10.1021/jp304564x.

[50] A. Heintz, J.K. Lehmann, S.A. Kozlova, E.V. Balantseva, A.B. Bazyleva, D. Ondo, Micelle formation of alkylimidazolium ionic liquids in water and in ethylammonium nitrate ionic liquid: a calorimetric study, Fluid Phase Equilib. 294 (2010) 187–196, https://doi.org/10.1016/j.fluid.2010.01.022.

[51] G.S. Kell, Effects of isotopic composition, temperature, pressure, and dissolved gases on the density of liquid water, J. Phys. Chem. Ref. Data. 6 (1977) 1109–1131, https://doi.org/10.1063/1.555561.

[52] Á. Piñeiro, E. Muñoz, J. Sabín, M. Costas, M. Bastos, A. Velázquez-Campoy, P.F. Garrido, P. Dumas, E. Ennifar, L. García-Río, J. Rial, D. Pérez, P. Fraga, A. Rodríguez, C. Cotelo, AFFINImeter: a software to analyze molecular recognition processes from experimental data, Anal. Biochem. 577 (2019) 117–134, https://doi.org/10.1016/j.ab.2019.02.031.

[53] R.M.A. Azzam, N.M. Bashara, Ellipsometry and Polarized Light, North Holland, Amsterdam, 1977.

[54] D. Langevin, Light Scattering by Liquid Surfaces and Complementary Techniques, CRC Press, New York, 1991, pp. 333–364.

[55] A. Tummino, J. Toscano, F. Sebastiani, B.A. Noskov, I. Varga, R.A. Campbell, Effects of aggregate charge and subphase ionic strength on the properties of spread polyelectrolyte/surfactant films at the air/water interface under static and dynamic conditions, Langmuir 34 (2018) 2312–2323, https://doi.org/10.1021/acs.langmuir.7b03960.

[56] R.A. Campbell, H.P. Wacklin, I. Sutton, R. Cubitt, G. Fragneto, FIGARO: the new horizontal neutron reflectometer at the ILL, Eur. Phys. J. Plus. 126 (2011) 107, https://doi.org/10.1140/epjp/i2011-11107-8.

[57] L. Braun, M. Uhlig, R. von Klitzing, R.A. Campbell, Polymers and surfactants at fluid interfaces studied with specular neutron reflectometry, Adv. Colloid Interface Sci. 247 (2017) 130–148, https://doi.org/10.1016/j.cis.2017.07.005.

[58] A. Nelson, Co-refinement of multiple-contrast neutron/X-ray reflectivity data using MOTOFIT, J. Appl. Crystallogr. 39 (2006) 273–276, https://doi.org/10.1107/S0021889806005073.

[59] L.G. Parratt, Surface studies of solids by total reflection of x-rays, Phys. Rev. 95 (1954) 359–369, https://doi.org/10.1103/PhysRev.95.359.

[60] V. Lauter-Pasyuk, Neutron grazing incidence technique for nanoscience, Collect. La Société Française La Neutron. 7 (2007) 221–240, https://doi.org/10.1140/sfn:2007024.

[61] V.B. Fainerman, E.V. Aksenenko, S.V. Lylyk, A.V. Makievski, F. Ravera, J.T. Petkov, J. Yorke, R. Miller, Adsorption layer characteristics of Tritons surfactants, Colloids Surfaces A Physicochem. Eng. Asp. 334 (2009) 16–21, https://doi.org/10.1016/j.colsurfa.2008.10.042.

[62] V.B. Fainerman, E.V. Aksenenko, S.A. Zholob, J.T. Petkov, J. Yorke, R. Miller, Adsorption layer characteristics of mixed SDS/CnEOm, solutions. II. dilational viscoelasticity, Langmuir 26 (2010) 1796–1801, https://doi.org/10.1021/la9024926.

[63] V.B. Fainerman, V.I. Kovalchuk, E.V. Aksenenko, M. Michel, M.E. Leser, R. Miller, Models of two-dimensional solution assuming the internal compressibility of

adsorbed molecules: a comparative analysis, J. Phys. Chem. B 108 (2004) 13700–13705, https://doi.org/10.1021/jp049120+.

[64] E.V. Aksenenko, V.I. Kovalchuk, V.B. Fainerman, R. Miller, Surface dilational rheology of mixed surfactants layers at liquid interfaces, J. Phys. Chem. C 111 (2007) 14713–14719, https://doi.org/10.1021/jp073904g.

[65] C. Monteux, G.G. Fuller, V. Bergeron, Shear and dilational surface rheology of oppositely charged polyelectrolyte/surfactant layers at the air-water interface. influence on foam stability, J. Phys. Chem. B 108 (2004) 16473–16482, https://doi.org/10.1021/jp047462.

[66] V.B. Fainerman, S.V. Lylyk, E.V. Aksenenko, N.M. Kovalchuk, V.I. Kovalchuk, J.T. Petkov, R. Miller, Effect of water hardness on surface tension and dilational visco-elasticity of sodium dodecylsulfate solutions, J. Colloid Interface Sci. 377 (2012) 1–6, https://doi.org/10.1016/j.jcis.2012.03.030.

[67] Y.-P. Huang, L. Zhang, L. Zhang, L. Luo, S. Zhao, J.-Y. Yu, Dynamic interfacial dilational properties of hydroxy-substituted alkyl benzenesulfonates, J. Phys. Chem. B 111 (2007) 5640–5647, https://doi.org/10.1021/jp070997t.

[68] D.J. Burgess, N.O. Sahin, Interfacial rheological and tension properties of protein films, J. Colloid Interface Sci. 189 (1997) 74–82, https://doi.org/10.1006/jcis.1997.4803.

[69] G. Espinosa, D. Langevin, Interfacial shear rheology of mixed polyelectrolyte-surfactant layers, Langmuir 25 (2009) 12201–12207, https://doi.org/10.1021/la901730f.

[70] A. Selmani, A. Tavera-Vázquez, C. Garza, R. Castillo, Tuning the viscoelastic-gel transition of single-wall carbon nanotubes embedded in pH-responsive polyelectrolyte solutions, J. Phys. Chem. B 122 (2018) 348–359, https://doi.org/10.1021/acs.jpcb.7b09112.

[71] A. Tavera-Vázquez, B. Arenas-Gómez, C. Garza, Y. Liu, R. Castillo, Structure, rheology, and microrheology of wormlike micelles made of PB–PEO diblock copolymers, Soft Matter. 14 (2018) 7264–7276, https://doi.org/10.1039/C8SM01530A.

[72] K. Tonigold, I. Varga, T. Nylander, R.A. Campbell, Effects of aggregates on mixed adsorption layers of poly(ethylene imine) and sodium dodecylsulfate at the air/liquid interface, Langmuir 25 (2009) 4036–4046, https://doi.org/10.1021/la8028325.

[73] H. Nakayama, K. Shinoda, The effect of added alcohols on the solubility and the krafft, J. Phys. Chem. 70 (1966) 3502–3504, https://doi.org/10.1021/j100883a022.

[74] B.G. Mathapa, V.N. Paunov, Cyclodextrin stabilised emulsions and cyclodextrinosomes, Phys. Chem. Chem. Phys. 15 (2013) 17903, https://doi.org/10.1039/c3cp52116h.

[75] B.G. Mathapa, V.N. Paunov, Self-assembly of cyclodextrin–oil inclusion complexes at the oil–water interface: a route to surfactant-free emulsions, J. Mater. Chem. A 1 (2013) 10836, https://doi.org/10.1039/c3ta12108a.

[76] L. Jiang, Y. Peng, Y. Yan, M. Deng, Y. Wang, J. Huang, "Annular Ring" microtubes formed by SDS@2β-CD complexes in aqueous solution, Soft Matter. 6 (2010) 1731, https://doi.org/10.1039/b920608f.

[77] L. Jiang, Y. Peng, Y. Yan, J. Huang, Aqueous self-assembly of SDS@2β-CD complexes: lamellae and vesicles, Soft Matter. 7 (2011) 1726–1731, https://doi.org/10.1039/C0SM00917B.

[78] S. Yang, Y. Yan, J. Huang, A.V. Petukhov, L.M.J. Kroon-Batenburg, M. Drechsler, C. Zhou, M. Tu, S. Granick, L. Jiang, Giant capsids from lattice self-assembly of cyclodextrin complexes, Nat. Commun. 8 (2017) 15856, https://doi.org/10.1038/ncomms15856.

[79] B.G. Mathapa, V.N. Paunov, Fabrication of novel cyclodextrin-polyallylamine hydrochloride co-polymeric microcapsules by templating oil-in-water emulsions, Soft Matter. 9 (2013) 4780, https://doi.org/10.1039/c3sm27935a.

[80] B.G. Mathapa, V.N. Paunov, Nanoporous cyclodextrin-based co-polymeric microspheres for encapsulation of active components, J. Mater. Chem. B 1 (2013) 3588–3598, https://doi.org/10.1039/c3tb20481b.

[81] B.G. Mathapa, V.N. Paunov, Fabrication of viable cyborg cells with cyclodextrin functionality, Biomater. Sci. 2 (2014) 212–219, https://doi.org/10.1039/C3BM60162E.

[82] F. Hapiot, H. Bricout, S. Menuel, S. Tilloy, E. Monflier, Recent breakthroughs in aqueous cyclodextrin-assisted supramolecular catalysis, Catal. Sci. Technol. 4 (2014) 1899–1908, https://doi.org/10.1039/c4cy00005f.

[83] F. Hapiot, S. Menuel, E. Monflier, Thermoresponsive hydrogels in catalysis, ACS Catal. 3 (2013) 1006–1010, https://doi.org/10.1021/cs400118c.

[84] K. Ito, Slide-ring materials using cyclodextrin, Chem. Pharm. Bull. 65 (2017) 326–329, https://doi.org/10.1248/cpb.c16-00874.